Dynamic Response of a Wind Farm Consisting of Doubly-Fed Induction Generators to Network Disturbance

Temitope Raphael Ayodele, Abdul-Ganiyu Adisa Jimoh, Josiah Munda, and John Agee

Department of Electrical Engineering, Tshwane University of Technology, Pretoria, South Africa
{AyodeleTR,JimohAA,MundaJL,AgeeJT}@tut.ac.za

Abstract. In this paper, the response of a wind farm consisting of doubly fed induction generators when a disturbance occurs on the network is studied. The disturbances include occurrence of fault on the network, the sudden change in load, loss of transmission line and loss of generation. The influence of generator inertial and fault location on the dynamics of the generator is also considered. First, the mathematical model comprising the variable speed wind conversion system is established. Based on this model, the simulation results describing the behaviour of a wind farm consisting of doubly fed induction generators to different network disturbances are presented.

Keywords: Wind Farm, Doubly Fed Induction Generator, Power System, Disturbance.

1 Introduction

Wind power has proven to be a renewable energy source that is sustainable for electricity generation with lower impact on the environment. The rapid development in wind energy technology and the reduction in wind power production costs have increased its rate of integration into the grid around the world in recent years. At present, the wind power growth rate stands at over 20% annually. At the end of 2010, global cumulative wind power capacity reached 194.4 GW [1] and it is predicted that 12% of the world electricity may come from wind power by the year 2020 [2]. The global exponential growth of wind power cumulative capacity in the last 15 years is depicted in Fig.1.

There are various types of wind turbines in use around the world each having its own advantages and disadvantages [3]. The most used one is the variable speed wind turbine with doubly fed induction generator (DFIG) due to the numerous advantages it offers over others [4]. The stator of DFIG is directly connected to the grid while the rotor is coupled to the grid through a Pulse Width Modulation (PWM) frequency converter. One of the attractive characteristics of this generator is that the converter carries only the rotor slip power typically in the range of 10-15% of the generated power [5]. The reduced rating of the converter reduces the cost and the power losses,

N. Pina et al. (Eds.): *Simulation & Modeling Methodologies, Technologies & Appl.*, AISC 197, pp. 131–150.
DOI: 10.1007/978-3-642-34336-0_9

the annual energy capture is in the range of 20–30% higher than the fixed speed wind generator [6] . The use of capacitor banks is eliminated because it has both active and reactive power control capability which also enhances its contribution to voltage and load flow distribution control in the power system. The lower mechanical stress imposed by DFIG on the gearbox extends the life span of this expensive device. The controllability of the speed makes it possible to use aerodynamic pitch control, which effectively limits the generated power during high wind speed periods. Flickers caused by the aerodynamic torque oscillation and the wind gust are greatly reduced thereby improving the power quality of the network.

Until quite recently, the power system mainly consisted of the synchronous generators. The behaviour and the characteristic of these conventional generators to network disturbance are generally well understood by the utility operators. With the advent of wind power, induction generator technologies are introduced into the power system. This poses a lot of concern to most utility operators as the response of these generators to network disturbance is not well understood.

Most existing literature is focused on the analysis of the behavior of power system networks as a result of wind farm integration [4, 7-9]. In this paper, however, the behaviour of a wind farm as a result of disturbance in the power system network is the subject of study. The study is limited to Wind farm (WF) consisting of variable speed DFIGs.

The rest of the paper is organized as follows; section two presents the model of the wind conversion system made of variable speed DFIG. In section three, the system under study is described. Simulation results obtained are discussed in section four while section five presents the conclusions.

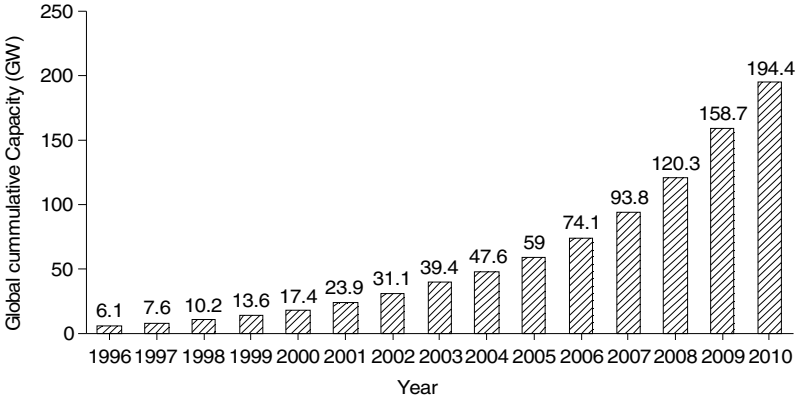

Fig. 1. Source: Adapted from [1]

2 Modelling of DFIG Wind Conversion System

Wind conversion system (WCS) comprises of the aerodynamic system, the mechanical shaft system, electrical system of the induction generator, the pitch control system, the speed control system, the rotor side converter controller and the grid side converter controller. All these systems are combined together to form a unit system of a wind farm as depicted in Fig 2.

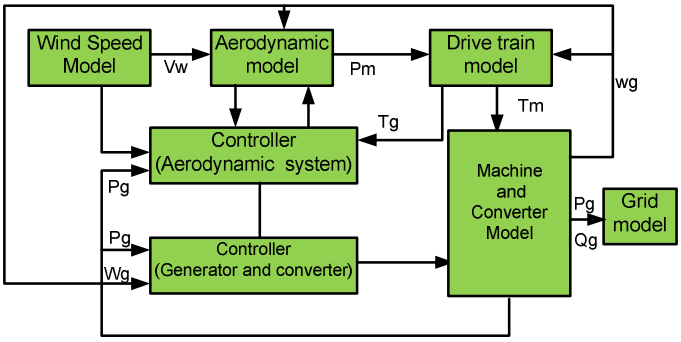

Fig. 2. Generic model of a DFIG

2.1 Aerodynamic Torque Model

Aerodynamic model involves the extraction of useful mechanical power from the available wind power. Available wind power is given by

$$P_{wind} = \frac{1}{2}\rho\pi R^2 V^3 \tag{1}$$

where P_{wind}, ρ, R and V are the available power in the wind, air density (kg/m^2), radius of the turbine blade (m) and the wind speed (m/s) that reaches the rotor swept area (m^2). The fraction of wind power that is converted to the turbine mechanical power P_m is given by

$$P_m = \frac{1}{2}\rho\pi R^2 C_p(\lambda,\beta) V^3 \tag{2}$$

where C_p gives the fraction of available wind power that is converted to turbine mechanical power, λ and β are the tip speed ratio and the pitch angle respectively. The C_p, λ and β are related by equation (3) and (4) [10]

$$C_p(\lambda,\beta) = c_1\left(\frac{c_2}{\lambda_i} - c_3\beta - c_4\right)e^{\frac{c_5}{\lambda_i}} + c_6\lambda \tag{3}$$

$$\frac{1}{\lambda_i} = \frac{1}{1+0.08\beta} - \frac{0.035}{\beta^2+1} \tag{4}$$

Given $c_1 = 0.5176$, $c_2 = 116, c_3 = 0.4, c_4 = 5, c_5 = 21$ and $c_6 = 0.0068$,the relationship between C_p against λ at various β is given in figure 3.

The tip speed ratio is given by (5)

$$\lambda = \frac{R\omega t}{V} \tag{5}$$

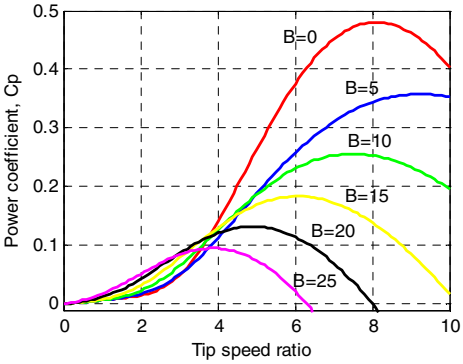

Fig. 3. Relationship between Power coefficient and tip speed ratio at different pitch angle

The mechanical torque (Nm) developed by the wind power is given by (6)

$$T_{ma} = \frac{P_m}{\omega_t} = \frac{\frac{1}{2}\rho\pi R^2 C_p(\lambda,\beta)V^3}{\omega_t} \tag{6}$$

where ω_t is the turbine speed.

2.2 Maximum Power Tracking of Variable Speed Wind Turbine

In the time when the wind speed is in the range of cut-in and rated value, the maximum aerodynamic power available in the wind can be capture. The maximum power in a mass of wind can be extracted by varying the turbine speed with the varying wind speed so that at all times it is on the track of the maximum power curve [6].

For efficient wind power captured by the variable wind turbine [11], $\lambda = \lambda_{opt}$, therefore (5) can be re-written as (7)

$$V = \frac{R\omega t}{\lambda_{opt}} \tag{7}$$

substituting (7) in (2), optimum power can be obtained as (8) which can be re-written as (9)

$$P_{opt} = \frac{1}{2}\frac{\rho\pi R^5 C_p(\lambda_{opt},\beta=0)\omega t^3}{\lambda_{opt}^3} \tag{8}$$

$$P_{opt} = k_{opt}\omega t^3 \tag{9}$$

where,

$$k_{opt} = \frac{1}{2}\frac{\rho\pi R^5 C_p(\lambda_{opt},\beta=0)}{\lambda_{opt}^3}$$

Fig 4 depicts the maximum power tracking of a variable speed wind turbine at different wind speed.

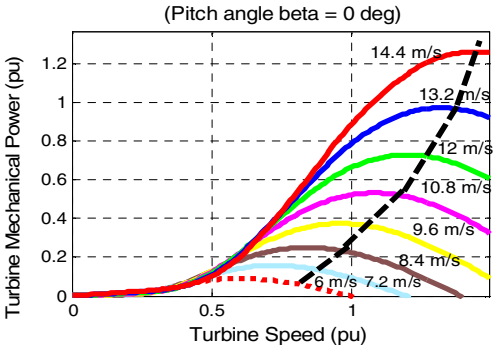

Fig. 4. Maximum torque tracking of a variable speed wind turbine

2.3 The Mechanical Shaft System Model

Adequate model of the mechanical drive train is required when the study involves the response of a system to heavy disturbances. It is better to represent the shaft by at least two- mass model [12] as show in Fig 5 where the turbine is coupled to the generator through a gearbox.

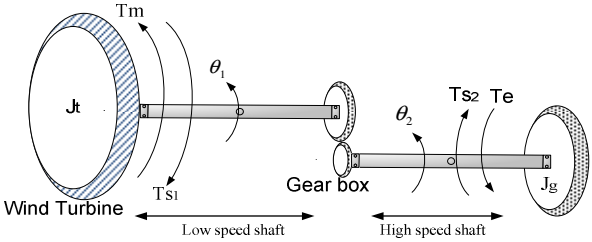

Fig. 5. Two mass model of the mechanical shaft system

From the figure, the following equations can be derived (10)-(17)

$$2H_t \frac{d\omega_t}{dt} = T_m - Ts_1 \tag{10}$$

$$2Hg \frac{d\omega_r}{dt} = Ts_2 - T_e \tag{11}$$

Where,

$$H_g = \frac{J_g \omega^2}{2n_p{}^2 P_g} \text{ and } H_T = \frac{J_T \omega^2}{2n^2 P_g} \tag{12}$$

$$Ts_1 = K_1\theta_1 + F_1\frac{d\theta_1}{dt} \text{ and } Ts_2 = K_2\theta_2 - F_2\frac{d\theta_2}{dt} \tag{13}$$

$$\theta_{eq} = \theta_1 - \theta_2, K_{eq} = \frac{K_1 * K_2}{K_1 + K_2} \text{ and } T_{eq} = \frac{Ts_1 * Ts_2}{Ts_1 + Ts_2} \tag{14}$$

$$T_{eq} = K_{eq}\theta_{eq} + F_{eq}\frac{d\theta_{eq}}{dt} \tag{15}$$

$$\frac{d\theta_{eq}}{dt} = \omega_t - \omega_r \tag{16}$$

$$\frac{\mathrm{d}\theta_{\mathrm{eq}}}{\mathrm{dt}} = \omega_{\mathrm{t}} - \omega_{\mathrm{r}} \tag{17}$$

where H_t, Hg are the pu turbine and generator inertia respectively. J_g and J_T are the inertia in kgm^2. T_e is the electromechanical torque developed by the induction generator, T_m is the pu mechanical torque applied to the turbine by the wind derived from (6). Ts_1, Ts_2, T_{eq} are the torques developed by the shaft at the low speed side, torque developed by the shaft at the high speed side and the equivalent torque developed by the shafts respectively. ω_t and ω_r are the pu turbine and generator rotor speed. K_1, K_2 and K_{eq} are shaft stiffness at low speed side, shaft stiffness at high speed side and the total shaft stiffness. F_1, F_2 and F_{eq} are the damping coefficient of the shaft at the low speed side, high speed side and the equivalent damping coefficient of the shaft respectively. θ_1, θ_2 and θ_{eq} are the angle of twist of the shaft at low speed, high speed and the equivalent angle of twist of the shaft respectively. n_p is the number of pole pairs, n is the gear ratio, P_g is the generator active power, ω is $2\pi f$ where f is the frequency (Hz).

2.4 Pitch Angle Controller Model

Pitch angle controller mainly serves the purpose of limiting the generated power to the rated power at time of high wind speed. It also limits the speed of the generator during heavy disturbances. The pitch controller based on PI is given by (18) [13]

$$\begin{aligned} \frac{d\beta}{dt} &= \frac{1}{\tau_s}\left(\beta_{ref} - \beta\right) \\ \beta_{ref} &= \left(k_P + \frac{k_i}{s}\right)\left(P_{ref} - P_m\right) \end{aligned} \tag{18}$$

where β_{ref} is the reference pitch control, k_P and k_i are the proportional and integral parameters of the PI controller, P_{ref} is the reference turbine power.

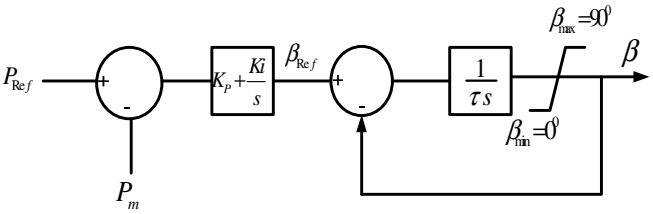

Fig. 6. Pitch angle controller

2.5 Wind Generator Model

Most wind farms are made of induction generators because they are cheap and robust. The dq stator and rotor voltage equations model in generating mode are as follows [14, 15].

$$v_{qs} = -r_s i_{qs} - \omega\lambda_{qs} - p\lambda_{qs} \tag{19}$$

$$v_{ds} = -r_s i_{ds} + \omega\lambda_{qs} - p\lambda_{ds} \tag{20}$$

$$v_{qr} = -r_r i_{qr} - (\omega - \omega_r)\lambda_{qr} - p\lambda_{qr} \tag{21}$$

$$v_{dr} = -r_r i_{dr} + (\omega - \omega_r)\lambda_{qr} - p\lambda_{dr} \tag{22}$$

where r_s , r_r are the stator and rotor speed resistance, p is $\frac{d(.)}{dt}$ term.

The equation presented in (19)–(22) is a fifth order model. Third order model is obtained by neglecting the transient term in the stator voltage equation. The stator and rotor flux equations are

$$\lambda_{qs} = L_s i_{qs} + L_m i_{qr} \tag{23}$$

$$\lambda_{ds} = L_s i_{ds} + L_m i_{dr} \tag{24}$$

$$\lambda_{qr} = L_r i_{qr} + L_m i_{qs} \tag{25}$$

$$\lambda_{dr} = L_r i_{dr} + L_m i_{ds} \tag{26}$$

where L_s , L_r , L_m are the stator, rotor and magnetizing inductance respectively. i_{ds} , i_{qs} i_{dr} and i_{qr} are the stator and rotor d-axis and q-axis current.

The electromechanical torque, T_e developed by the induction generator in pu can be derived as (27)

$$T_e = \frac{1}{\sigma}\left(\lambda_{qs}\lambda_{dr} - \lambda_{qr}\lambda_{ds}\right) \tag{27}$$

where

$$\sigma = 1 - \frac{L_m^2}{L_r L_s}$$

The equation is completed by the mechanical coupling equation in pu between the turbine and the generator using two mass model as derived in (10)–(15)

$$\frac{d\omega_r}{dt} = \frac{1}{2H_g}\left(Ts_2 - T_e\right) \tag{28}$$

the active and reactive power generated by the induction generator is given as

$$P_s = \frac{3}{2}\left(v_{qs}i_{qs} + v_{ds}i_{ds}\right) \tag{29}$$

$$Q_s = \frac{3}{2}\left(v_{qs}i_{ds} - v_{ds}i_{qs}\right) \tag{30}$$

2.6 Grid Connection of DFIG

DFIG technology makes use of wound rotor. The stator is directly connected to the grid while the rotor is coupled to the grid through a PWM) frequency converter as shown in Fig. 7.

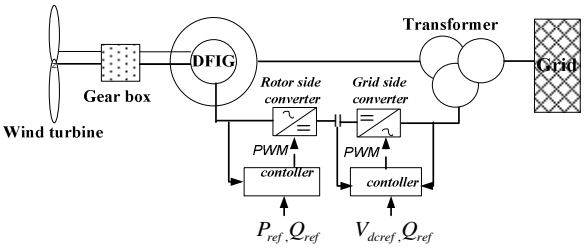

Fig. 7. DFIG with PWM converter control system

For dynamic study of DFIG, the converter controller model is important. Stator flux oriented control is commonly used in the decoupled control of DFIG.

2.7 DFIG Rotor Side Converter Controller

The control of the DFIG rotor is done in a synchronous rotating reference frame i.e. $\omega = \omega_e$ in equation (18)-(21). The rotor side converter controls the stator active and reactive power of the DFIG. By aligning the d-q reference frame in the stator flux reference frame as in figure 8 [16], then $v_{ds} = 0$ $v_{qs} = v_s$, $\lambda_{ds} = \lambda_s$ and $\lambda_{qs} = 0$.

From (25) and (26)

$$i_{qs} = -\frac{L_m}{L_s} i_{qr} \tag{31}$$

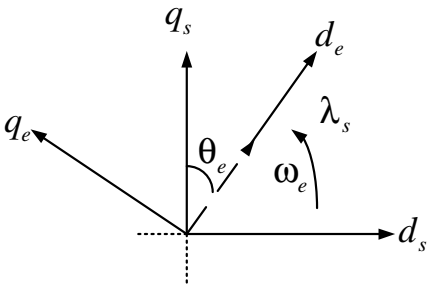

Fig. 8. Stator flux vector orientation along the rotating reference frame

Substituting (31) in (29) and (30) with vector control and re-arranging, we obtain (32) and (33)

$$P_s = -\frac{3}{2}\frac{L_m}{L_s} v_s i_{qr}^* \tag{32}$$

$$Q_s = \frac{3}{2L_s}\left(\frac{v_s^2}{\omega_s} - v_s L_m i_{dr}^*\right) \tag{33}$$

The rotor voltage equation governing the active and reactive power control can be obtained by rearranging equation (19)–(26) and is given by (34) and (35)

$$v_{dr} = r_r i_{dr} + \sigma L_r \frac{d}{dt} i_{dr} - (\omega_e - \omega_r)(\sigma L_r i_{qr}) \tag{34}$$

$$v_{qr} = r_r i_{qr} + \sigma L_r \frac{d}{dt} i_{qr} + (\omega_e - \omega_r)\sigma L_r i_{dr} + (\omega_e - \omega_r)\frac{L_m}{L_s}\lambda_{ds} \tag{35}$$

Where

$$\sigma = 1 - \frac{L_m^2}{L_r L_s}$$

Equations (34) and (35) can be rewritten as (36) and (37) to form the decoupled control of active and reactive power.

$$v_{dr}^* = \left(k_{dp} + \frac{k_{di}}{s}\right)\left(i_{dr}^* - i_{dr}\right) - \left(\omega_e - \omega_r\right)\sigma L_r i_{qr} \tag{36}$$

$$v_{qr}^* = \left(k_{qp} + \frac{k_{qi}}{s}\right)\left(i_{qr}^* - i_{qr}\right) - \left(\omega_e - \omega_r\right)(\sigma L_r i_{dr} - \frac{L_m}{L_s}\lambda_s) \tag{37}$$

where, k_{dp}, k_{di} are the PI proportional and integral constant for the d-axis for the control of reactive power while gain k_{qp}, k_{qi} are the PI constant for controlling the active power. i_{qr}^* and i_{dr}^* are the reference current for the active and reactive power

respectively. v_{dr}^{*} and v_{qr}^{*} are the d-q reference voltage which will be converted to a-b-c frame to generate command for the rotor end PWM converter. The block diagram is shown in figure 9.

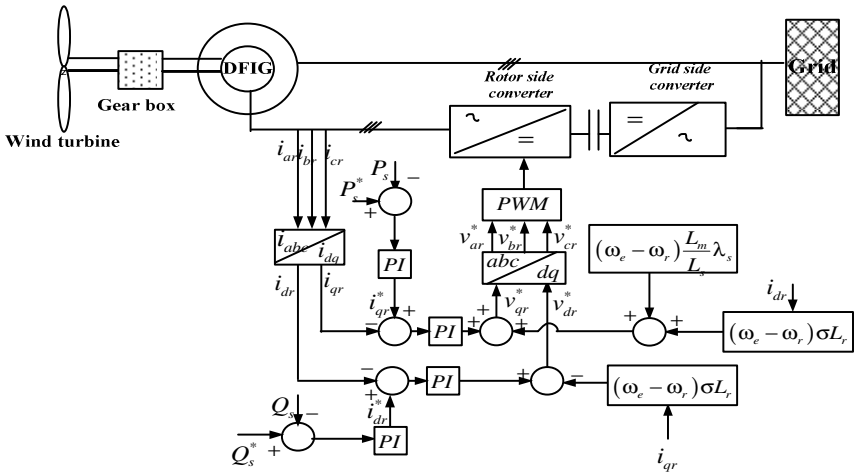

Fig. 9. Rotor side Controller system

2.8 DFIG Grid Side Converter Controller

The main objective of grid side controller is to maintain the dc link between the back to back PWM converters at constant voltage irrespective of the direction of power flow [14]. The voltage for the grid side converter is represented by (38) [17]

$$\begin{bmatrix} v_{as} \\ v_{bs} \\ v_{cs} \end{bmatrix} = r \begin{bmatrix} i_{as} \\ i_{bs} \\ i_{cs} \end{bmatrix} + L\frac{d}{dt}\begin{bmatrix} i_{as} \\ i_{bs} \\ i_{cs} \end{bmatrix} + \begin{bmatrix} v_{a1} \\ v_{b1} \\ v_{c1} \end{bmatrix} \tag{38}$$

The d-q transformation of equation (38) yields (39)

$$\begin{aligned} v_q &= Ri_q + L\frac{di_q}{dt} + \omega_e L_{id} + v_{q1} \\ v_d &= Ri_d + L\frac{di_d}{dt} - \omega_e L_{iq} + v_{d1} \end{aligned} \tag{39}$$

Re-arranging (39) with $v_{qs} = 0$, the governing voltage equation for the grid side converter can be obtained as (40)

$$\begin{aligned} v_{q1}^{*} &= -\left(k_{1p} + \frac{k_{1i}}{s}\right)\left(i_q^{*} - i_q\right) - \omega_e L_{id} \\ v_{d1}^{*} &= -\left(k_{2p} + \frac{k_{2i}}{s}\right)\left(i_d^{*} - i_d\right) + \omega_e L_{iq} + v_d \end{aligned} \tag{40}$$

where k_{1p} , k_{1i} are the q axis PI proportional and the integral constant k_{2p} , k_{2i} are the d axis PI proportionality and integral constant respectively. v_{q1}^{*} and v_{d1}^{*} are the reference voltages that generate the command for the grid side PWM converter after conversion to abc frame. i_q^{*} is derived from the grid reactive power error while i_d^{*} is derived from the dc link voltage error as shown in Fig.10.

Applying the grid voltage oriented control i.e. aligning the d axis of the reference frame along the grid voltage vector, then $v_q = 0$.

Hence, active and reactive power can be written as (41) and (42)

$$P_g = \frac{3}{2} v_d i_d \tag{41}$$

$$Q_g = -\frac{3}{2} v_d i_q \tag{42}$$

The reactive power can be controlled by the i_q of the grid side converter. The energy stored in the dc link can be written as (43).

$$\frac{1}{2} c v_{dc}^2 \tag{43}$$

Where c and v_{dc} are the dc link capacitor and voltage respectively

$$c v_{dc} \frac{d}{dt} v_{dc} = P_g - P_r \tag{44}$$

$$c \frac{d}{dt} v_{dc} = \frac{P_g}{v_{dc}} - \frac{P_r}{v_{dc}} = i_{og} - i_{or} \tag{45}$$

where

$$i_{og} = \frac{3}{2} \frac{v_d}{v_{dc}} i_d$$

$$\frac{v_d}{v_{dc}} = \frac{m}{\sqrt[2]{2}} \tag{46}$$

where m is the modulation factor which gives the ratio of grid voltage to the dc bus voltage [18].

$$c \frac{d}{dt} v_{dc} = \frac{3m}{\sqrt[4]{2}} i_d - i_{or} \tag{47}$$

Hence, i_d can be used for the control of dc bus voltage.

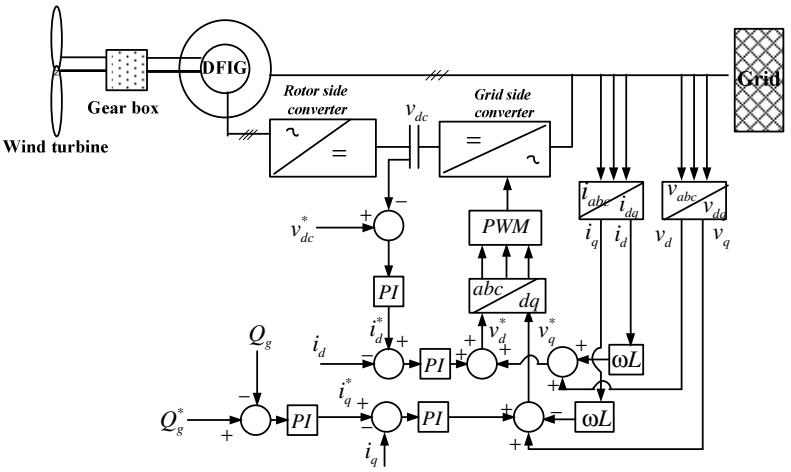

Fig. 10. Grid side controller system

2.9 Protection of Converter (Crowbar Protection)

High currents due to a fault close to the generator can damage the rotor side converter. To avoid any damages, the rotor side converter is bypassed when the rotor current exceeds a predetermined limit. To achieve this, an additional resistance otherwise known as "crowbar" is connected to the rotor circuit. The thyristors are turned on when the rotor current exceeds its preset value. The rotor circuits are then short-circuited by the crowbar and it shunts away the rotor overcurrent. Fig 11 shows a crowbar protection system where r_{cr} is the additional resistance added for crowbar protection. The rotor remains connected to the crowbar until the fault is cleared.

When crowbar protection is initiated as a result of rotor current exceeding the set limit, then $v_{dr} = v_{qr} = 0$, hence the DFIG operates as normal singly fed induction generator.

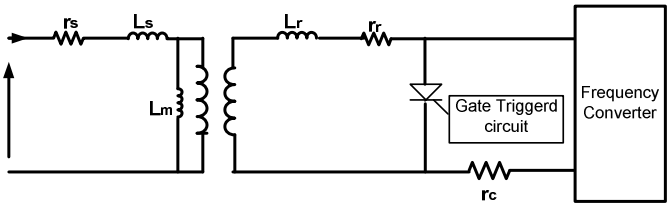

Fig. 11. Crowbar protection circuit

From the diagram the rotor voltage equation (21) and (22) will be modified to (48) and (49)

$$0 = (r_r + r_c) i_{dr} + \frac{d}{dt}\lambda_{dr} - (\omega_e - \omega_r)\lambda_{qr} \tag{48}$$

$$0 = (r_r + r_c) i_{qr} + \frac{d}{dt}\lambda q_r - (\omega_e - \omega_r)\lambda_{dr} \tag{49}$$

2.10 Wind Farm Model

Combinations of several WCS constitute a WF and simulation of complete wind farm with large numbers of WCS will be computationally intensive without much difference in the assessment. Aggregate model reduces simulation time required by detailed multi turbines system [19-21].The objective is to represent a large wind farm with many WCS by a single turbine system[22]. The following criteria must be fulfilled when reducing a large wind farm into an aggregate model assuming a regular wind distribution [19, 22]

1. The MVA rating of the equivalent WF S_{wf} is the sum of individual MVA rating of the WCS

$$S_{wf} = \sum_{i=1}^{n} S_i \tag{50}$$

where S_i is the MVA rating of WCS, i and n are the numbers of WCS in the WF

2.

$$P_{wf} = \sum_{i=1}^{n} P_i \tag{51}$$

Where P_{wf} is the electric power supplied by the equivalent WF, P_i is the electric power supply by i^{th} WCS.

3. The dynamics of the wind generators are given by the slope of the $P-Q$ characteristics of the induction generator.

$$\frac{dQ}{dP_{wf}} = \sum_{i=1}^{n} \frac{dQ}{dP_i} \tag{52}$$

Where dQ/dP_{wf} is the $P-Q$ characteristic of the equivalent WF and dQ/dP_i is the i^{th} $P-Q$ characteristic of the WCS.

3 System under Study

The system considered for the study is shown in Fig. 12. It consists of 110MW, 50MVAR synchronous generator (SG) connected to bus 4 through a 20/400kV transformer.

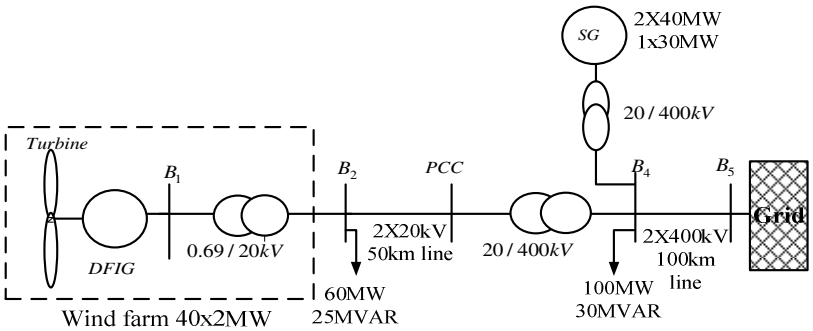

Fig. 12. The system under study

The wind farm (WF) is made up of 40 wind turbines of 2MW, 0.69kV each modelled as an aggregate wind turbine. It is assumed that the wind farms are located far from the point of common connection (PCC) where the wind resources are abundantly located as the case for most real wind farms. The WF is connected to the PCC through two 20km line (to allow disconnection of a line) and 69/20KV transformer. The WF is feeding a 60MW, 25MVAR local load connected to bus2 (B2). Another 100MVA, 30MVAR load is connected to the high voltage bus (B4). The whole system is connected to a strong grid through a two 400kV, 100km transmission lines.

4 The Simulation Results and Discussions

Different scenarios were created to get an insight into the response of WF to disturbances from the grid. First, the response of the wind farm was studied when there is a step change of 20% in the local load connected to B_2 at 1s. The results with the rotor controller in place and out of place are depicted in Fig 13. From the figure it can be observed that with the controller in place, the active power (the negative values indicate a power injected into the grid) and the electrical torque are immediately returned to the pre-disturbance level. The step increase in the local load resulted in a dip in the terminal voltage and an increase in the speed of the generator; however, it stabilizes to a new value almost immediately. This is as a result of a change in the system configuration. With the rotor controller out, the system is stable but it takes about 3s for the wind farm to stabilize.

Fig. 14 shows the response of i_{dr} , i_{qr} , crowbar protection and the pitch angle (β) to a 20% step increase in local load. With this disturbance, the maximum i_{dr} current reaches 0.71pu from the prefault value of 0.65pu. The crowbar protection was set to operate at 1.5pu and therefore could not be inserted as the rotor current is lower than the crowbar predetermined value. The pitch angle controller acts to limit the speed of the generator as a result of the disturbance.

The response of the wind farm to a 3 phase fault of 200ms duration was investigated. The fault was created at 1s at the middle of 100km, 400kV line. The results of the response of the DFIG speed, the electrical torque, voltage at the point of common connection (PCC) and the pitch controller are presented in Fig 15. The speed of the generator is limited by the pitch angle. The first swing of the DFIG speed reached a value of 1.26pu from the prefault value of 1.21pu. The fault causes a dip in voltage at the PCC, the pitch controller acts to stabilize the speed of the generator.

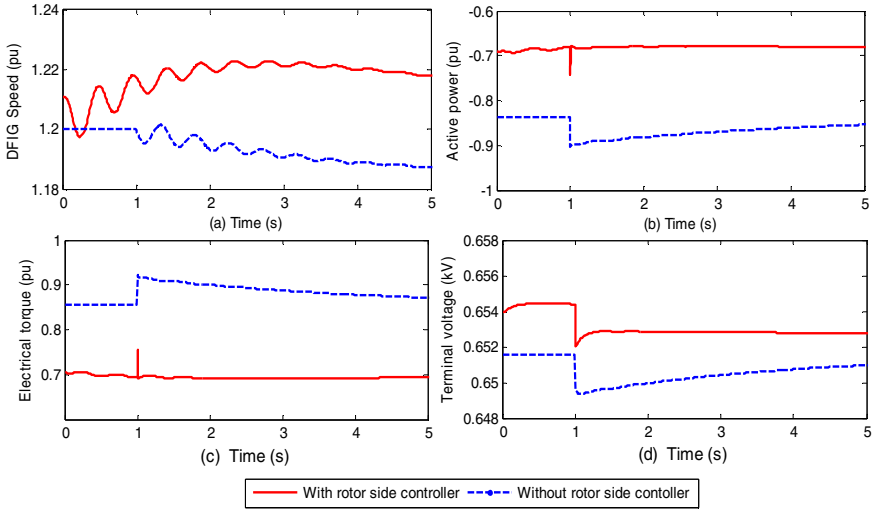

Fig. 13. The response of (a) DFIG speed (b) Active power, (c) Electrical torque (d) Terminal voltage to 20% step change in local load at 1s

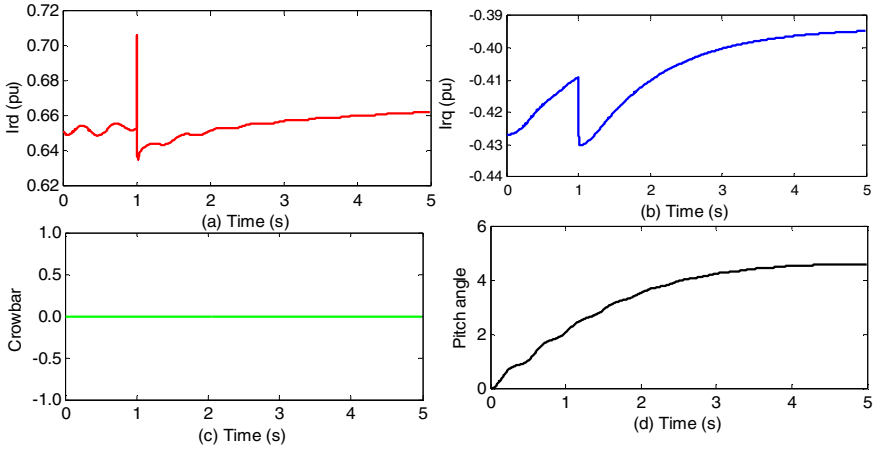

Fig. 14. The response of (a) Rotor d-axis current (b) Rotor q-axis current (c) Crowbar protection (d) Pitch controller when a step change of 20% is initiated in the local load at 1s

Figure 16 depicts the rotor d-axis current, rotor q-axis current, the rotor current and the crowbar protection. The rotor current reached 2pu during the fault which initiated the operation of the crowbar protection so as to prevent damage to the converter.

The response of the wind farm to different fault locations was examined. To get an insight into this scenario, a three phase fault of 200ms duration was created at different locations on the 50km, 20kV line. The result is shown in Fig. 17. From the result, the impact of fault at different locations has almost the same impact on the response of the wind farm. However, the impact is visibly different at the PCC. The closer the fault location to the PCC, the more the dip in voltage and the more the deviation from the nominal grid frequency.

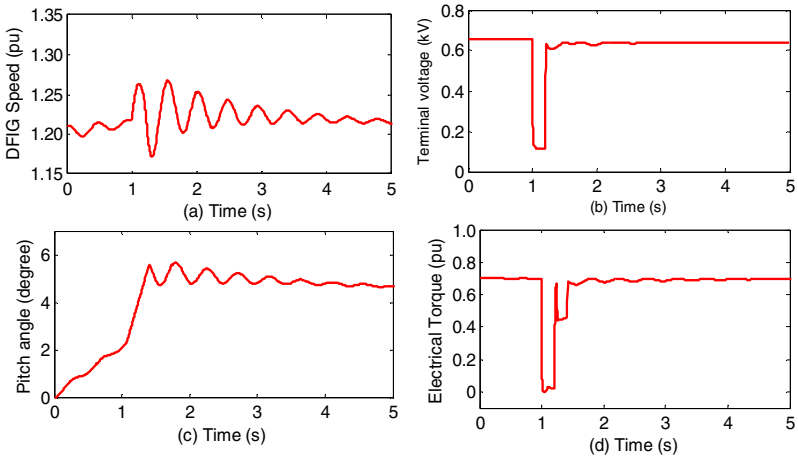

Fig. 15. Response of the Wind farm (a) speed (b) PCC voltage (c) pitch controller (d) Electrical torque when a three phase fault of 200ms duration is created at 1s at the middle of 100 km, 400kV line

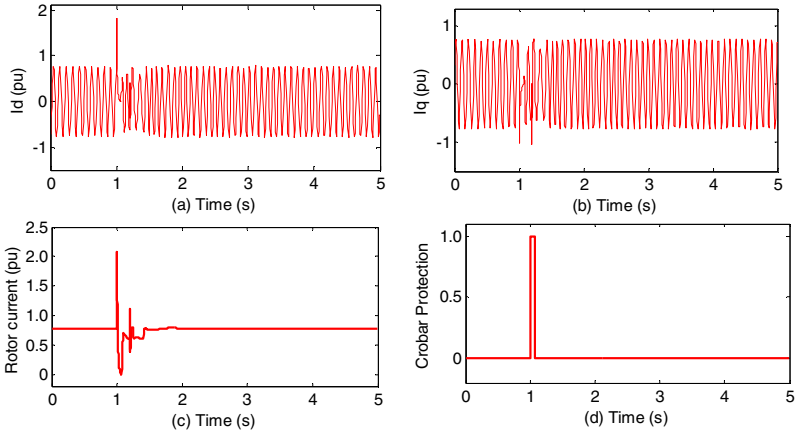

Fig. 16. (a) The rotor d-axis current (b) rotor q-axis current (c) the rotor current (d) the crowbar protection when a three phase fault of 200ms duration is created at 1s at the middle of 100 km, 400kV line

Fig. 18 shows the response of the wind generator with different rotor inertia to a three phase fault created at the middle of 400kV line. The effect of inertia can be noticed in the speed of the generator. The generators with larger inertia are more stable in case of fault compared to the generator with smaller inertia. The first swing in rotor speed for 50kgm^2 is 1.28pu, 1.26pu for 100kgm^2, 1.24pu for 150kgm^2 and 1.22pu for 200kgm^2. No distinct differences in the response of the active power, electrical torque and the terminal voltage are seen.

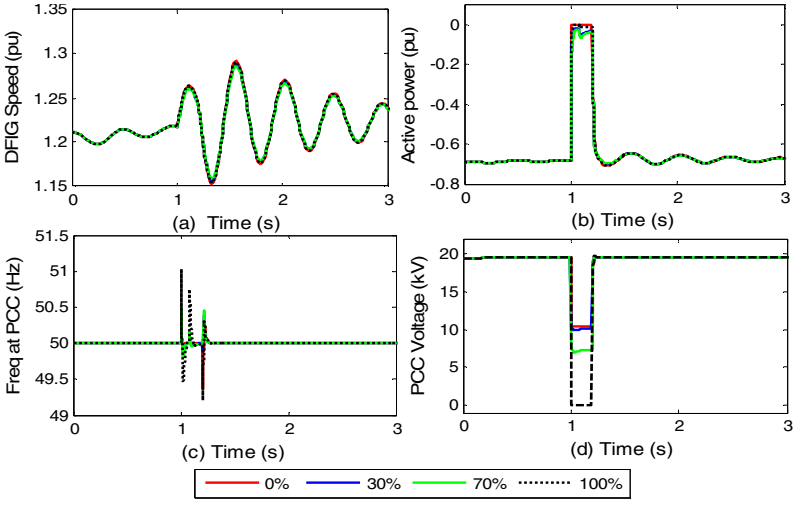

Fig. 17. Response of (a) DFIG speed (b) DFIG active power (c) PCC frequency and (d) PCC voltage to 3 phase fault (200ms duration) at different locations on the 20kV line

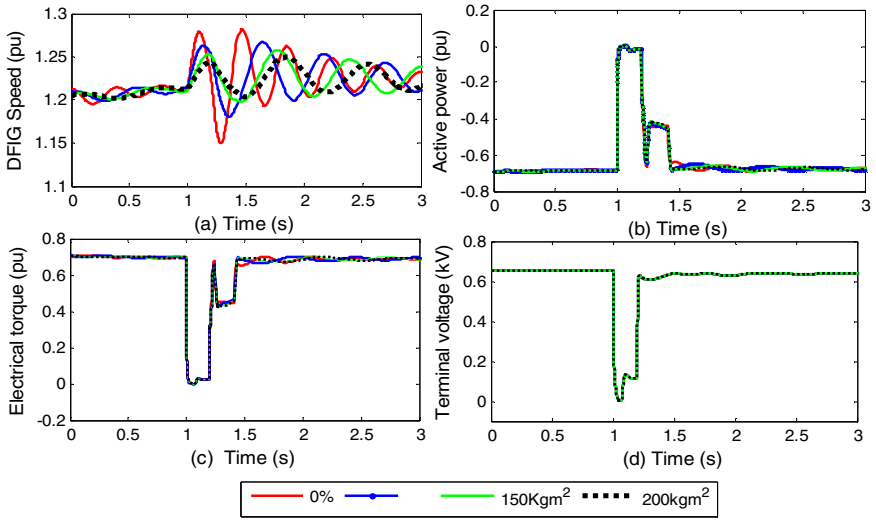

Fig. 18. Wind farm with DFIG of different inertia

The effect of a loss of transmission line (TL) and generation on the behaviour of the WF was studied. For the TL, the circuit breakers at both ends of the lines were opened at 1s for the 400kV, 100km line and then for 20kV, 50km line in turn. The circuit breaker at bus 4 connecting the synchronous generator (SG) to the grid was opened at 1s to disconnect the SG from the power system. The results are shown in Fig 19. A loss of line causes a surge in the system frequency at the PCC; this caused a reduction of active power to the network by the WF to restore the frequency to the prefault value. The 20kV, 50km line has a severe impact compared to the 400kV, 100km line due to close proximity to the WF. At the instant the SG (generation) was lost; a sudden dip in the system frequency was experienced, this in turn resulted into an instant injection of active power from the WF to the grid to restore the system frequency.

The terminal voltage reduces from the prefault value of 0.655kV to a new value of 0.638kV, 0.641kV and 0.650kV for the loss of 50km line, 100km line and SG respectively as a result of change in the system configuration.

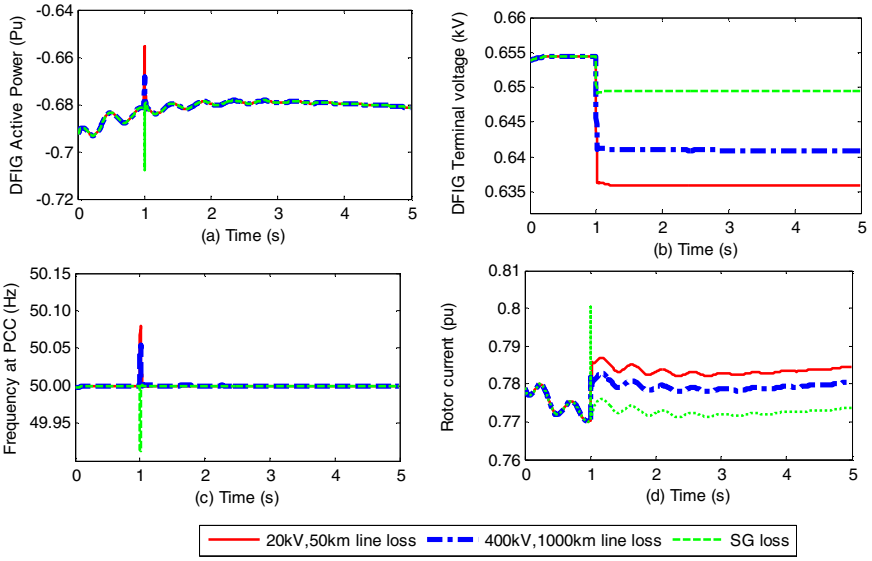

Fig. 19. Response to loss of transmission line

5 Conclusions

The behaviour of a wind farm consisting of DFIG in response to different disturbances emanating from the power system has been studied. From the study, the effect of the rotor controller on the stability of a wind farm has been shown to be significant to the stability of the wind farm following a disturbance. Without controller, prefault condition was achieved after about 3s. With a controller, the prefault condition was achieved almost immediately.

The location of the fault occurrence is seen to have little effect on the wind farm. However the location of fault occurrence has significant effect on the frequency and the voltage at the PCC.

The inertia of wind generators has influence on the response of the WF to a disturbance. The larger the inertia the lower the magnitude of oscillation of the generator speed. A larger inertia enhances good stability. The WF responds to the sudden loss of transmission line and generation in such a way as to restore the system frequency. The rotor current and the terminal voltage assume a new value due to the change in the network configuration.

This paper is useful to the utility operators in understanding the probable response of a wind farm during disturbance in the power system. However, a qualitative study mainly is carried out on a small test system. Further investigation is necessary for a large power system.

References

1. GWEC, Global Wind Statistic (2010), http://www.gwec.net
2. El-Sayed, M.A.: Integrating Wind Energy into Weak Power Grid Using Fuzzy Controlled TSC Compensator. In: International Conference on Renewable Energies and Power Quality (ICREPQ 2010), Granada, Spain (2010)
3. Slootweg, J.G., De Haan, S.W.H., Polinder, H., Kling, W.L.: Modeling wind turbines in power system dynamics simulations. In: Power Engineering Society Summer Meeting, vol. 1, pp. 22–26. IEEE (2001)
4. Xing, Z., Zheng, Q., Yao, X., Jing, Y.: Integration of Large Double-Fed Wind Power Generator System into Grid. In: 8th International Conference on Electrical Machines and System, pp. 1000–1004 (2005)
5. Veganzones, C., Martinez, S., Blazquez, F.: Large Scale Integration of Wind Energy into Power Systems. Electrical Power Quality and Utilisation, Magazine 1, 15–22 (2005)
6. Seul-Ki, K., Eung-Sang, K., Jae-Young, Y., Ho-Yong, K.: PSCAD/EMTDC based dynamic modeling and analysis of a variable speed wind turbine. In: IEEE Power Engineering Society General Meeting, vol. 2, pp. 1735–1741 (2004)
7. Eping, C., Stenzel, J., Poller, M., Muller, H.: Impact of Large Scale Wind Power on Power System Stability. In: 5th International Workshop on Large-Scale Integration of Wind Power and Transmission Networks for Offshore Wind Farms, Glasgow, Scoland (2005)
8. Folly, K.A., Sheetekela, S.: Impact of fixed and variable speed wind generators on the transient stability of a power system network. In: Power Systems Conference and Exposition, PSCE 2009, pp. 1–7. IEEE/PES (2009)
9. Naimi, D., Bouktir, T.: Impact of Wind Power on the Angular Stability of a Power System. Leonardo Electronic Journal of Practices and Technologies 12, 83–94 (2008)
10. El-Sayed, M.A., Adel, M.S.: Wind Energy-Grid Stabilization using a Dynamic Filter Compensator. In: International Conference on Renewable and Power Quality (ICRPQ 2010), Spain (2010)
11. Arifujjaman, M.D., Iqbal, M.T., Quaicoe, J.E.: Vector Control of a DFIG Based Wind Turbine. Journal of Electrical & Electronics Engineering 9, 1057–1066 (2009)
12. Poller, M.A.: Doubly_FEd Induction Machine Models for Stability Assessment of Wind Farms, http://www.digsilent.de/consulting/publication/DFIGmodelling (date accessed September 28, 2009)

13. El-Sattar, A.A., Saad, N.H., El-Dein, M.Z.S.: Dynamic Response of Doubly Fed Induction Generator Variable Speed Wind Turbine Under Fault. Electric Power Systems Research 78, 1240–1246 (2008)
14. Krause, P.C., Wasynczuk, O., Sudhoff, S.D.: Analysis of Electric Machinery and Drive Systems Second Edition. A John Wiley and Sons, Inc. Publication (2002)
15. Lipo, T.A.: Electric Machine Analysis and Simulation, Wisconsin Power Electronic Research Center. University of Wisconsin-Madison, Madison (2000)
16. Simoe, M.G., Farret, F.A.: Renewable Energy Systems: Design and Analysis with Induction Generators. CRC Press, Boca Raton (2004)
17. Soares, O.M., Gocalves, H.N., Martins, A.P., Carvalho, A.: Analysis and NN-Based Control of Doubly Fed Induction Generator in Wind Power Generation. In: International Conference on Renewable Energies and Power Quality (ICREPQ 2009), Valencia, Spain (2009)
18. Salman, S.K., Badrzadeh, B.: New Approach for Modelling Doubly-Fed Induction Genertaor (DFIG) for Grid-Connected Studies. In: European Wind Energy Conference and Exhibition, pp. 1–13 (2004)
19. Akhmatov, V.: An Aggregate Model of a Grid-connected, Large-scale, Offshore Wind Farm for Power Stability Investigations- Importance of Windmill Mechanical system. Electric Power and Energy Systems 24, 709–717 (2002)
20. Conroy, J., Watson, R.: Aggregate Modelling of Wind Farms Containing Full-Converter Wind Turbine Generators with Permanent Magnet Synchronous Machines. Transient Stability Studies. IET Renewable Power Generation 3, 39–52 (2009)
21. Poller, M., Achilles, S.: Aggregated Wind Park Models for Analyzing Power System Dynamics. In: 4th International Workshop on Large- Scale Integration of Wind Power and Transmission Networks for Off-shore Wind Farms, Billund, Denmark (2003)
22. Zhao, S., Nair, N.C.: Behavior of Doubly - Fed Induction Generator Unit during System Disturbance. In: Australasian Universities Power Engineering Conference, AUPEC 2008, pp. 1–6 (2008)